Study of beamstrahlung effects at CEPC*

Qing-Lei Xiu (修青磊)[1,2;1)] Hong-Bo Zhu (朱宏博)[1,2;2)] Teng Yue (岳腾)[2,3]
Xin-Chou Lou (娄辛丑)[1,2,4]

[1] State Key Laboratory of Particle Detection and Electronics, Beijing 100049, China
[2] Institute of High Energy Physics, CAS, Beijing 100049, China
[3] University of Chinese Academy of Sciences, Beijing 100049, China
[4] University of Texas at Dallas, Richardson, TX 75080-3021, USA

Abstract: The discovery of a 125 GeV Higgs boson at the LHC marked a breakthrough in particle physics. The relative lightness of the new particle has inspired consideration of a high-luminosity Circular Electron Positron Collider (CEPC) as a Higgs Factory to study the particle's properties in an extremely clean environment. Given the high luminosity and high energy of the CEPC, beamstrahlung is one of the most important sources of beam-induced background that might degrade the detector performance. It can introduce even more background to the detector through the consequent electron-positron pair production and hadronic event generation. In this paper, beamstrahlung-induced backgrounds are estimated with both analytical methods and Monte Carlo simulation. Hit density due to detector backgrounds at the first vertex detector layer is found to be $\sim$0.2 hits/cm^2 per bunch crossing, resulting in a low detector occupancy below 0.5%. Non-ionizing energy loss (NIEL) and total ionizing dose (TID), representing the radiation damage effects, are estimated to be $\sim10^{11}$ 1 MeV $n_{\rm eq}$/cm^2/yr and $\sim$300 kRad/yr, respectively.

Keywords: CEPC, beamstrahlung, pair production, detector backgrounds, radiation damage

PACS: 29.20.db, 29.27.-a, 25.20.Lj **DOI:** 10.1088/1674-1137/40/5/053001

1 Introduction

Since the Higgs boson was discovered by the ATLAS and CMS experiments [1, 2] at the CERN Large Hadron Collider (LHC), it has become a matter of urgency to measure the particle properties with high precision, which is even beyond the ultimate reach of the LHC [3, 4]. This goal is generally believed to be only achievable at future lepton colliders (so-called "Higgs Factories"), e.g. the Circular Electron Positron Collider (CEPC) [5] proposed by the Chinese high energy physics community. The CEPC machine will primarily operate at the center-of-mass energy of 240–250 GeV (near the ZH production threshold) with an instantaneous luminosity of 2×10^{34} cm$^{-2}\cdot$s^{-1} at two interaction points (IP). To achieve such high luminosity, both electron and positron beams must be heavily squeezed to very small section sizes right before collision. As a consequence, the trajectories of the electrons/positrons in each bunch will be bent significantly by the electromagnetic field that is formed by the beam particles of the opposite charge inside the crossing bunch. During this process, a particular kind of synchrotron radiation, called "beamstrahlung" [6], will be emitted. Consequent processes including electron-positron pair production and hadronic event generation [7], both of which involve the energetic beamstrahlung photons, are considered among the most important detector backgrounds at the CEPC and their impact must be carefully evaluated.

2 Analytical estimation of the beamstrahlung backgrounds

Beamstrahlung can be characterised by the parameter Υ :

$$\Upsilon=\frac{2}{3}\frac{\hbar\omega_c}{E} \tag{1}$$

where $\hbar\omega_c=\frac{3}{2}\hbar\gamma^3c/\rho$ denotes the critical energy of synchrotron radiation, ρ the bending radius of the charged particle trajectory, γ the Lorentz factor of the beam particles, and E the beam particle energy before radia-

Received 11 May 2015, Revised 14 January 2016

∗ Supported by CAS/SAFEA International Partnership Program for Creative Research Teams, CAS and IHEP Thousand Talent and Hundred Talent programs, and grants from the State Key Laboratory of Nuclear Electronics and Particle Detectors.

1) E-mail: xiuql@ihep.ac.cn

2) E-mail: zhuhb@ihep.ac.cn

tion. The higher the Υ, the more beamstrahlung photons with higher energies will be emitted. Assuming Gaussian charge distributions inside the two colliding beams, the average Υ can be estimated with the following formula:

$$\Upsilon_{\rm av} \approx \frac{5}{6}\frac{Nr_{\rm e}^2\gamma}{\alpha(\sigma_x+\sigma_y)\sigma_z} \quad (2)$$

where $r_{\rm e}$ is the classical electron radius, α the fine structure constant, σ_x/σ_y the transverse size of the bunch and σ_z the bunch length [8].

With the machine parameters of LEP2 [9], CEPC [5], FCC-ee [10] and ILC [11], as listed in Table 1, the average beamstrahlung parameters $\Upsilon_{\rm av}$ of these colliders are calculated with Eq. 2. The bunch sizes ($\sigma_{x,y,z}$) of CEPC, FCC-ee and ILC are expected to be significantly smaller than those of LEP2, leading to non-negligible beamstrahlung effects. Nevertheless the bunch sizes of CEPC and FCC-ee are much larger than those of ILC and the beamstrahlung effects will be accordingly smaller.

Table 1. Machine parameters of LEP2, CEPC, FCC-ee and ILC and their average beamstrahlung parameters $\Upsilon_{\rm av}$ calculated with Eq. (2).

parameters	symbol	LEP2	CEPC	FCC-ee	ILC250
center of mass energy	$E_{\rm cm}$/GeV	209	240	240	250
bunch population	$N/\times10^{10}$	58	37.1	37	2
horizontal beam size at IP	σ_x/nm	270000	73700	61000	729
vertical beam size at IP	σ_y/nm	3500	160	120	7.7
bunch length	σ_z/μm	16000	2260	2110	300
horizontal beta function at IP	β_x/mm	1500	800	500	13
vertical beta function at IP	β_y/mm	50	1.2	1	0.41
normalized horizontal emittance at IP	$\gamma\epsilon_x$/(mm·mrad)	9.81	1594.5	1761.3	10
normalized vertical emittance at IP	$\gamma\epsilon_y$/(mm·mrad)	0.051	4.79	3.52	0.035
luminosity	$L/(10^{34}\ {\rm cm}^{-2}\cdot{\rm s}^{-1})$	0.013	1.8	5.08	0.75
beamstrahlung parameter	$\Upsilon_{\rm av}$ $[\times10^{-4}]$	0.25	4.7	6.1	200
relative average energy loss per BX due to beamstrahlung	$\delta_{\rm av}$ [%]	0.0001	0.005	0.0075	1.0

2.1 Beamstrahlung photons

Assuming Gaussian charge distributions in the two colliding bunches, the average number of photons n_γ emitted by each beam particle in one bunch crossing (BX) can be approximated with:

$$n_\gamma \approx 2.59\left(\frac{\alpha\sigma_z}{\lambda_{\rm e}\gamma}\Upsilon_{\rm av}\right)\frac{1}{(1+\Upsilon_{\rm av}^{2/3})^{1/2}} \quad (3)$$

where $\lambda_{\rm e}$ is the electron Compton wavelength [8]. Given the CEPC beam parameters, there would be merely ∼0.22 photons emitted by each individual electron/positron. However the total number of photons per bunch crossing can become significant because of the large bunch population of 3.71×10^{11}.

2.2 Pair production

There are two kinds of processes for pair creation in beam-beam interactions, namely coherent and incoherent pair production. In coherent pair production, a real photon converts into an electron-positron pair in the strong macroscopic electromagnetic field formed by the crossing bunch. The total number of coherent pairs in each bunch crossing can be estimated with:

$$n_{\rm b} \approx \left(\frac{\alpha\sigma_z}{\gamma\lambda_{\rm e}}\Upsilon\right)^2\Xi(\Upsilon)$$

with

$$\Xi(\Upsilon)=\begin{cases}(7/128)\exp(-16/(3\Upsilon)) & (\Upsilon\lesssim1)\\ 0.295\Upsilon^{-2/3}(\ln\Upsilon-2.488) & (\Upsilon\gg1)\end{cases}. \quad (4)$$

Equation 4 suggests that coherent pair production with small Υ will be exponentially suppressed [8]. With $\Upsilon_{\rm av}=4.7\times10^{-4}$ for CEPC, the number of coherent pairs produced in each bunch crossing is very close to zero and has a negligible contribution to the detector backgrounds.

In incoherent pair production, an electron-positron pair is produced via the interaction between two incoming photons, which can be real and/or virtual. There are three incoherent processes, including: the Breit-Wheeler process $\gamma\gamma\to{\rm e^+e^-}$, in which both photons are real; the Bethe-Heitler process $e\gamma\to{\rm ee^+e^-}$, in which one photon is real and the other is virtual; and the Landau-Lifshitz process $ee\to{\rm eee^+e^-}$, in which both photons are virtual. The approximate cross sections of the three processes can be calculated with the formulae in Refs. [8, 12, 13]. In each bunch crossing at CEPC, there will be roughly 44, 327 and 1322 electron-positron pairs produced from the Breit-Wheeler process, the Bethe-Heitler process and the Landau-Lifshitz process, respectively.

2.3 Hadronic backgrounds

In addition to electron-positron pairs, two colliding photons can also produce hadrons. The cross section of the hadronic process, in units of nb, can be parameterised as [14]:

$$\sigma_{\rm H} = 211\left(\frac{s}{\rm GeV^2}\right)^{0.0808} + 297\left(\frac{s}{\rm GeV^2}\right)^{-0.4525} \quad (5)$$

where s is the square of the center-of-mass energy of the two colliding photons. The number of hadronic events produced in each bunch crossing at CEPC will be very small. A small fraction of the events could contain final state particles of high transverse momenta and have a potential impact on the calorimeter detector performance.

To summarize, the analytical estimation suggests that there will be a significant number of beamstrahlung photons produced in each bunch crossing at CEPC. The consequent incoherent electron-positron pair production represents an important source of detector background, while coherent pair production and hadronic events could be negligible. Nevertheless, to fully assess their impact on the CEPC detector, studies based on Monte Carlo simulation are performed below.

3 Simulation studies of the beamstrahlung backgrounds

Beam-beam interactions at CEPC have been simulated with Guinea-Pig++ (Generator of Unwanted Interactions for Numerical Experiment Analysis Program Interfaced to GEANT) [15], which allows detailed studies of the emission of beamstrahlung photons, incoherent pair production and hadronic events. In the Guinea-Pig++ simulation, the bunches are cut into slices in the longitudinal direction. Because the beam particles are ultra-relativistic, the electromagnetic field of both slices is flattened to a plane perpendicular to the beam direction. Thus, each slice interacts consecutively with each slice in the other bunch and interactions between two slices can be simplified as a two dimensional problem. Each slice is further cut into cells forming a grid in the transverse direction and the potentials on the grid points can be calculated according to the distribution of charge. The forces on beam particles can be derived from the potentials. In addition, the charge distributions in both colliding bunches are assumed to be Gaussian. The relevant configuration parameters are listed in Table 1. In order to reduce the simulation time, electron-positron pairs with energies less than 5 MeV are not tracked as they can be safely confined in the beam pipe with the solenoid magnetic field.

Background events generated with Guinea-Pig++ are interfaced to Mokka [16]/GEANT4 [17] for full detector simulation. Besides the direct contributions from the primary background particles, backgrounds from the secondary particles that are formed from the interactions of the primary background particles with detector materials should also be taken into account. The exact level of this background strongly depends on the detector layout and material distribution and will be extracted with detector simulation. Figure 1 shows the current design of the interaction region layout. The tracking system is composed of the vertex detector (VTX), the silicon tracker and the time projection chamber (TPC). The VTX consists of 6 layers of pixel detectors, which are assembled on both sides of 3 layers of mechanical support structures. An electromagnetic calorimeter (LumiCal) is designed to precisely measure the luminosity by counting the radiative Bhabha events. The final focusing magnets QD0 are placed at a short focal length of $L^* = 1.5$ m, *i.e.* the distance between the final quadrupole QD0 and the IP, to achieve high luminosity. Hit density and radiation damage, which are crucial parameters for detector design, are extracted based on this interaction region layout.

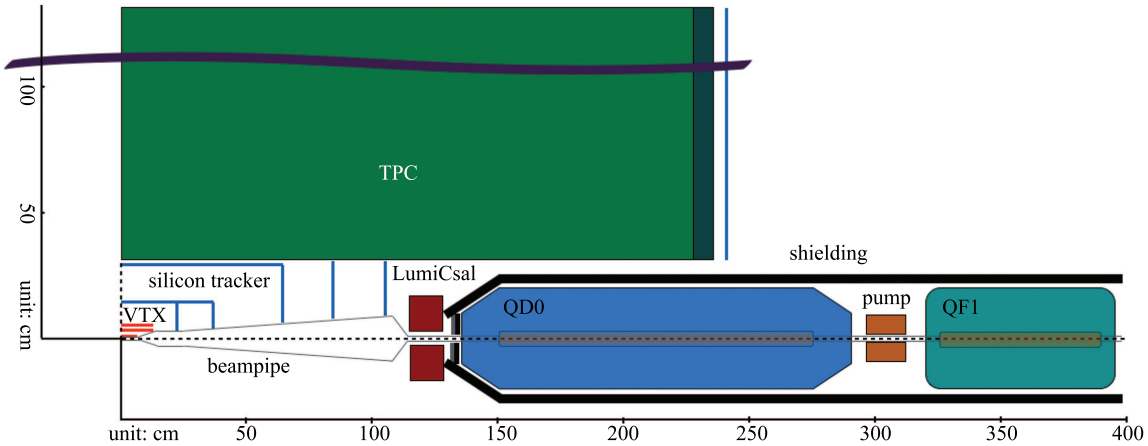

Fig. 1. (color online) A possible layout of the CEPC interaction region.

4 Simulation results

4.1 Beamstrahlung photons

Figure 2 shows the transverse momentum distribution versus the polar angle of the beamstrahlung photons originating from the beam-beam interactions. The photons are confined within a small angle of $|\theta| < 1$ mrad, so most of them will leave the interaction region without interacting with the beam pipe and will be negligible for the detector backgrounds.

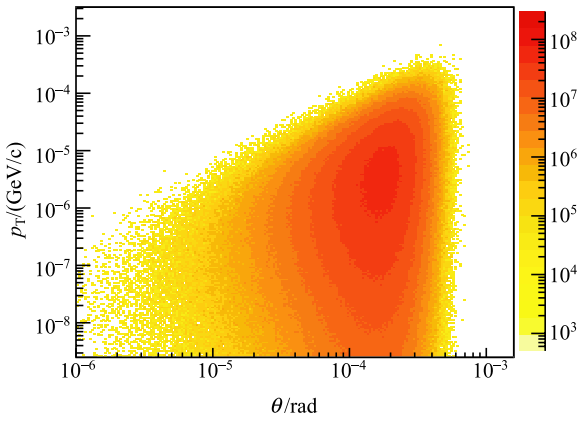

Fig. 2. (color online) p_T versus θ distribution of the beamstrahlung photons at the CEPC.

4.2 Incoherent electron-positron pairs

Unlike beamstrahlung photons, electrons and positrons from incoherent pair production are usually produced with large polar angle and high transverse momentum. They can contribute to the detector backgrounds in both direct and indirect ways:

1) If the primary particles are produced with large polar angles, they will hit the detector directly;

2) If the primary particles are produced with small polar angles, they might hit the beampipe or the detector components in the very forward region and produce secondary particles. Those particles can be back-scattered into the central region of the detector.

Figure 3 shows the p_T versus θ distribution of the electrons and positrons from incoherent pair production. The empty region at the bottom-right corner is formed because electrons/positrons with energy below 5 MeV are not tracked in the Guinea-Pig++ simulation. In Fig. 3, most of the electrons and positrons are concentrated in the area under an envelope (the so-called "kinematic edge"), which can be fitted to the following empirical formula:

$$p_T = 0.0202\, p_Z^{0.297} \tag{6}$$

Assuming perfect helical trajectories in a solenoidal magnetic field of 3.5 T, the charged particles along the envelope can develop a trajectory profile as shown in Fig. 4. The beam pipe (shown by the polyline) and any detector components must be kept sufficiently far away from the kinematic edge to avoid drastic particle showering.

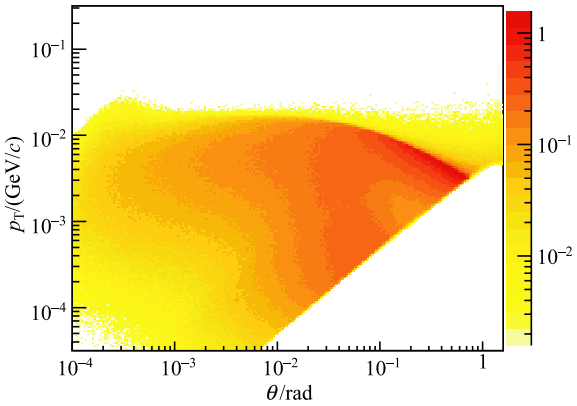

Fig. 3. (color online) p_T versus θ distribution of the electrons and positrons from incoherent pair production.

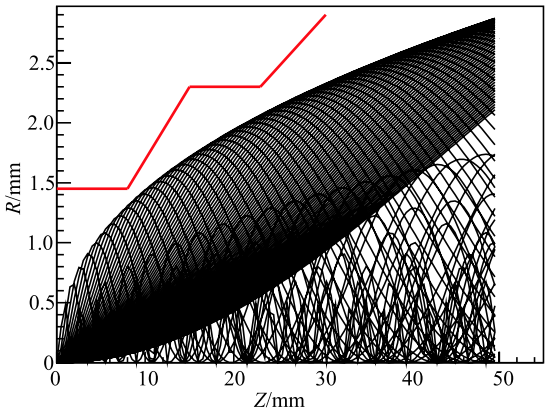

Fig. 4. (color online) The helical trajectories of electrons/positrons from pair production in a solenoidal magnetic field of 3.5 T. The polyline indicates the position of the beam pipe in the current design.

4.3 Hit density

Although most of the particles originating from beamstrahlung and consequent pair production will leave the interaction region without hitting the beam pipe, a small fraction of them will enter the detector directly, or hit the beam pipe and/or detector components in the forward region, which can introduce back-scattered particles. The resulting detector background will increase detector occupancy and cause radiation damage to silicon devices close to the interaction point.

The estimated hit densities at the 6 layers of the vertex detector (VTX) are shown together in Fig. 5. At the innermost VTX layer positioned at $r = 1.6$ cm, the hit

density is ∼0.2 hits/cm²/BX. With a bunch spacing of ∼ 3.6 μs for the current CEPC single-ring design, the resulting detector occupancy will be well below 0.5% for the first VTX layer, assuming a pixel pitch size of 20 μm and readout time of 20 μs.

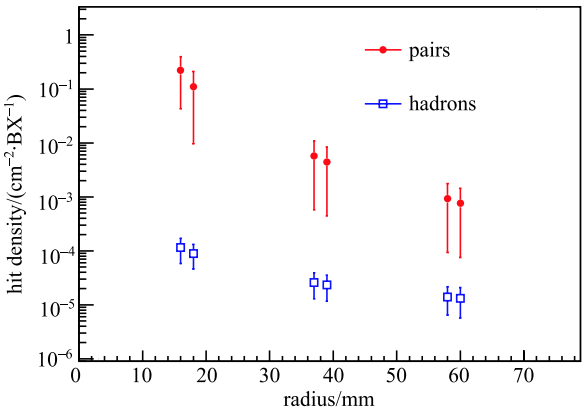

Fig. 5. (color online) Hit density of pairs and hadronic backgrounds at 6 layers of the VTX detector with radii 16 mm, 18 mm, 37 mm, 39 mm, 58 mm and 60 mm.

4.4 Radiation damage

Although the estimated hit density per bunch crossing is rather low, the potential detector radiation damage can be considerable given the high repetition frequency of the CEPC machine, i.e. $\sim 2.8\times10^5$ bunch crossings per second in the current design. The radiation damage to the CEPC sub-detectors, in particular the vertex detector close to the interaction point, should be carefully evaluated. The effects of radiation damage on the silicon detector can be roughly characterized as non-ionizing energy loss (NIEL) and total ionizing dose (TID).

NIEL can lead to crystal defects by displacing the silicon atoms out of their lattice sites (so-called "bulk damage") [18]. The effects induced by any particle with a given energy can be normalized to the equivalent damage caused by 1 MeV neutrons and denoted as $n_{\rm eq}$. In this study, the electron flux at a given point is obtained by tracking all the particles with the assumption of perfect helices. The total NIEL per year is calculated with the same method used in Ref. [19], assuming machine operation for 10^7 seconds (referred to as a "Snowmass Year"). In addition, a safety factor of 10 is used in the calculation to account for imperfect knowledge and uncertain issues of the machine design at its early stage. Figure 6 shows the NIEL distribution in the CEPC vertex detector. At the first vertex detector layer, the annual value for NIEL is about 10^{11} 1 MeV $n_{\rm eq}$/cm².

TID can introduce ionization at the Si-SiO_2 interface, leading to performance degration of silicon devices [20]. TID can be determined with:

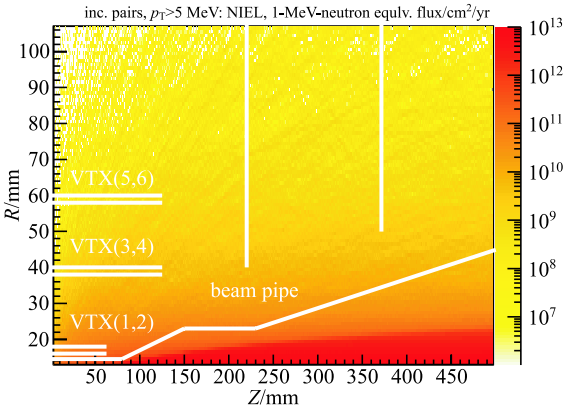

Fig. 6. (color online) NIEL distribution in the CEPC vertex detector. The white polyline and horizontal line segments indicate the positions of the beam pipe and the 6 VTX detector layers, respectively.

$$D=\frac{E_{\rm dep}}{m}=\frac{E_{\rm dep}}{\rho\cdot V}, \tag{7}$$

where $E_{\rm dep}$ is the energy deposited in the matter, and m, ρ and V are the mass, the density and the volume of the matter, respectively. These input parameters are extracted from the full detector simulation. In the TID calculation, a safety factor of 10 is also taken into account. The annual TID values at the 6 VTX detector layers are shown in Fig. 7 and the highest annual TID is found to be ∼300 kRad at the first vertex detector layer.

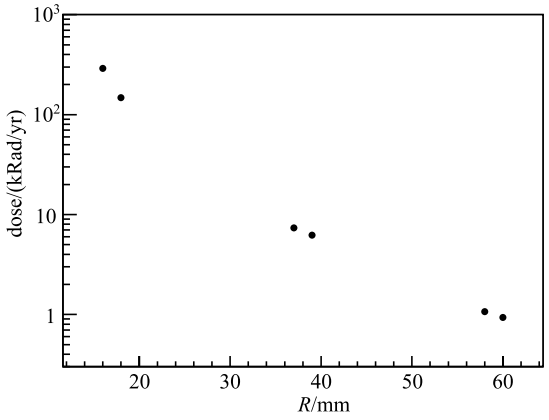

Fig. 7. TID at the vertex detector layers.

The potential radiation damage due to beamstrahlung and consequent pair production is found to be tolerable for most silicon detectors used in high energy physics experiments, but there are other backgrounds at circular electron-positron colliders, e.g. radiative Bhabha scattering and synchrotron radiation. Further investigations into these background sources are necessary to thoroughly understand the radiation tolerance requirements.

5 Conclusion

The backgrounds induced by beamstrahlung have been studied with both analytical and simulation methods. The average energy loss per bunch crossing due to beamstrahlung is small at the circular collider, thus its influence on physics analysis can be neglected. The hit density at the first vertex detector layer is only ∼0.2 hits/cm^2/BX and makes the detector occupancy well below 0.5%. The annual values for NIEL and TID, representing the levels of radiation damage in the silicon detectors, are estimated to be 10^{11} 1 MeV $n_{\rm eq}$/cm^2 and ∼300 kRad, respectively. Further studies on the beamstrahlung effects and other important sources of detector backgrounds, as well as detailed evaluation of their impacts on physics measurements, will be pursued in future.

The authors would like to thank WANG Dou, GENG Huiping and WANG Yiwei for fruitful discussions on accelerator physics, and MA Mingming for helping to generate simulation samples with large statistics.

References

1 G. Aad, T. Abajyan, B. Abbott et al, Phys. Lett. B, **716**: 1–29 (2012)
2 S. Chatrchyan, V. Khachatryan, A. M. Sirunyan et al, Phys. Lett. B, **716**: 30–61 (2012)
3 G. Aad, T. Abajyan, B. Abbott et al, ATLAS Notes, ATL-PHYS-PUB-2014–016 (2014)
4 S. Chatrchyan, V. Khachatryan, A. M. Sirunyan et al, CMS Notes, CMS-NOTE-13–002 (2013)
5 CEPC-SPPC Study Group, IHEP-CEPC-DR-2015-01, IHEP-AC-2015–01 (2015)
6 J. E. Augustin, N. Dikanski, Ya. Derbenev et al, in *Proceedings of the Workshop on Possibilities and Limitations of Accelerators and Detectors*, edited by D. A. Edwards (U.S. Government Printing Office, 1979), p.87
7 D. Schulte, *Study of electromagnetic and hadronic background in the interaction region of the TESLA Collider*, Ph.D. Thesis (University of Hamburg, 1997)
8 K. Yokoya, P. Chen, Lect. Notes Phys., **400**: 415–445 (1992)
9 V.I. Telnov, Phys. Rev. Lett., **110**: 114801 (2013)
10 M. Bicer, H. Duran Yildiz, I. Yildiz et al, JHEP, **01**: 164 (2014)
11 C. Adolphsen, M. Barone, B. Barish et al, ILC-REPORT-2013–040 (2013)
12 V. B. Berestetskii, E. M. Lifshitz and L. P. Pitaevskii, *Relativistic Quantum Theory* (Part 1. Pergamon Press, 1971)
13 V. N. Baier, E.A. Kuraev, V. S. Fadin et al, Phys. Rept., **78**: 293–393 (1981)
14 G. A. Schuler, T. Sjöstrand, Z. Phys. C, **73**: 677–688 (1997)
15 C. Rimbault, P. Bambade, O. Dadoun et al, in *Proceedings of PAC07* (Conf. Proc. C070625, 2007), p.2728
16 F. Gaede, J. Engels, EUDET-Report-2007–11 (2007)
17 S. Agostinelli, J. Allison, K. Amako et al, Nucl. Instrum. Methods A, **506**: 250–303 (2003)
18 R. C. Newman, Rep. Prog. Phys, **45**: 1163–1210 (1982)
19 Gunnar Lindstrom, Nucl. Instrum. Methods A, **512**: 30–43 (2003)
20 T. R. Oldham, F. B. McLean, Transactions on Nuclear Science, **50**(3): 483–499 (2003)